



HAL
open science

Development of an aqueous two-phase emulsion using hydrophobized whey proteins and erythritol

Ashkan Madadlou, Arnaud Saint-Jalmes, Fanny Guyomarc'H, Juliane Floury,
Didier Dupont

► **To cite this version:**

Ashkan Madadlou, Arnaud Saint-Jalmes, Fanny Guyomarc'H, Juliane Floury, Didier Dupont. Development of an aqueous two-phase emulsion using hydrophobized whey proteins and erythritol. *Food Hydrocolloids*, 2019, 93, pp.351-360. <10.1016/j.foodhyd.2019.02.031>. <hal-02024885>

HAL Id: hal-02024885

<https://hal.science/hal-02024885v1>

Submitted on 13 Mar 2019

HAL is a multi-disciplinary open access archive for the deposit and dissemination of scientific research documents, whether they are published or not. The documents may come from teaching and research institutions in France or abroad, or from public or private research centers.

L'archive ouverte pluridisciplinaire **HAL**, est destinée au dépôt et à la diffusion de documents scientifiques de niveau recherche, publiés ou non, émanant des établissements d'enseignement et de recherche français ou étrangers, des laboratoires publics ou privés.



Distributed under a Creative Commons CC BY-NC-ND 4.0 - Attribution - Non-commercial use - No Derivative Works - International License

Highlights

- Whey protein isolate (WPI) was hydrophobized by acetylation and heating
- Hydrophobized WPI and alginate were immiscible and formed W/W emulsions
- Erythritol addition to the WPI improved emulsification and emulsion stability
- Erythritol induced interactions between hydrophobized protein particles
- Furthermore, it decreased the air-water surface tension of WPI solution

1 Development of an aqueous two-phase emulsion using
2 hydrophobized whey proteins and erythritol
3
4

5 Ashkan Madadlou¹, Arnaud Saint-Jalmes², Fanny Guyomarc'h¹, Juliane Floury¹, Didier Dupont^{1*}
6

7 ¹ STLO, UMR 1253, INRA, Agrocampus Ouest, 35000 Rennes, France

8 ² Univ Rennes, CNRS, IPR (Institut de Physique de Rennes) - UMR 6251, F-35000 Rennes, France
9
10
11
12
13
14
15
16
17
18
19

20 -----
21 *Corresponding author, Email: didier.dupont@inra.fr
22

23 Abstract

24 Formation of aqueous two-phase (ATP) emulsions relies on the immiscibility of two
25 (bio)polymeric phases. Herein, we report that hydrophobization of whey proteins via a pre-
26 acetylation and succeeding acetylation/heating combined process makes solutions of whey
27 protein isolate (WPI) immiscible with alginate solutions. Erythritol was also added at different
28 concentrations (0, 52, 105, and 158 mg/g) into the hydrophobized WPI solution.
29 Subsequently, emulsions at an alginate to WPI weight ratio of 0.1 to 0.9 were prepared.
30 Erythritol supplementation facilitated emulsification and increased emulsion stability, so that
31 at the erythritol concentration of 105 mg/g, the emulsion was stable for a minimum duration
32 of 7 days. The droplet size evolved and reached to $\approx 5 \mu\text{m}$ during this period. The
33 hydrophobized protein had a mean hydrodynamic diameter of 80 nm, ζ -potential of -39 mV ,
34 and intrinsic fluorescence emission peak of 335 nm. Erythritol addition did not influence any
35 of the above-mentioned characteristics. However, the hydrophobized WPI solution changed
36 from Newtonian to a more viscous and shear-thinning fluid by adding erythritol at
37 concentrations $\geq 105 \text{ mg/g}$, due probably to the induction of interaction among protein
38 particles. A diameter of 150 nm was calculated for the air-dried hydrophobized protein
39 particles using atomic force microscopy images, supporting the assumption that exclusion of
40 erythritol from the protein particles surface induced inter-particle interactions. Erythritol
41 addition at 105 mg/g had a twofold larger influence on the surface tension of hydrophobized
42 WPI compared to water. It decreased the surface tension of hydrophobized WPI to 45 mN/m
43 after droplet ageing for 350 seconds.

44 **Keywords:** Emulsion; Whey protein; Water-in-water; Hydrophobicity.

45 1. Introduction

46 Aqueous two-phase (ATP) or water-in-water (W/W) emulsions consist of droplets of a
47 macromolecularly crowded aqueous solution, phase separated within a coexisting immiscible

48 aqueous phase (Dewey, Strulson, Cacace, Bevilacqua, & Keating, 2014). ATP emulsions can
49 be more biocompatible than oil-containing emulsions, because for instance the ATP
50 emulsions do not contain synthetic surfactant. The emulsions are increasingly used for diverse
51 objectives including bioactives delivery and synthesis of hydrogel particles (Song et al.,
52 2016). Recently, carboxymethyl cellulose droplets dispersed within a gelatin solution were
53 used for encapsulation of probiotic bacteria (Singh, Medronho, Miguel, & Esquena, 2018).

54 Thermodynamic incompatibility between two hydrophilic non-oppositely charged polymers
55 which causes immiscibility and segregative micro-phase separation (Esquena, 2016) is a
56 prerequisite to form ATP emulsions. It depends on variables such as pH value, ionic strength
57 (Grinberg & Tolstoguzov, 1997; Moschakis, Chantzou, Biliaderis and Dickinson, 2018) and
58 the difference between the hydrophilicity of the (bio)polymers (Grinberg & Tolstoguzov,
59 1997). The main drawback of ATP emulsions is their extremely low stability; the droplets
60 rapidly coalesce and the emulsion breaks down to macroscopically separated two layers
61 (Esquena, 2016). Stabilization of ATP emulsions is conventionally achieved through
62 emulsion gelation, so that the phase separation kinetics is arrested thanks to a fast gelation
63 rate of the continuous phase. Gelator precursors can be introduced into two immiscible
64 polymeric solutions to cause gelation when the solutions get in contact by mixing (Mytnyk et
65 al., 2017). Alternatively, interfacial accumulation of colloidal particles is used to stabilize
66 water-in-water emulsions without gelling the continuous phase (Nicolai & Murray, 2017). In
67 this approach, particles are added into the mixture of two incompatible polymer components
68 (Poortinga, 2008), partially partitioned into both phases (de Freitas, Nicolai, Chassenieux, and
69 Benyahia, 2016). Due to osmotic repulsion by both polymers, the particles are depleted from
70 the aqueous phases towards the interfacial boundary (Firoozmand, Murray, & Dickinson,
71 2009). Different types of particles including fat, latex, protein, liposomes, mineral platelets,
72 cellulose nanocrystals, and bacteria have been utilized for stabilization of ATP emulsions

73 (Ganley, Ryan, & van Duijneveldt, 2017). Finally, it is possible to enhance stability of ATP
74 emulsions by increasing the incompatibility between the two phases by varying the
75 hydrophilicities of the macromolecules and/or the quality of the aqueous solvent (Walstra,
76 2003). Modification of the chemical structure of proteins can influences their hydrophilicity
77 (Tyagi & Gupta, 1998) and allow to form ATP emulsions.

78 Chemical modification of proteins due to the wide array of available functional groups is easy
79 to perform and fascinating. It allows creating therapeutic conjugates and generating novel
80 constructs (Spicer & Davis, 2014). Recently, we hydrophobized whey proteins, a family of
81 food-grade and commercially available globular proteins, through a procedure that consisted
82 of pre-acetylation and subsequent acetylation/heating combined process (Madadlou, Floury,
83 Dupont, 2018). Herein, we report the applicability of the acetylated (hydrophobized) whey
84 proteins to form alginate-in-protein ATP emulsions. In such conditions, non-hydrophobized
85 whey proteins including native and heat-treated WPI (whey protein isolate) samples were
86 miscible with alginate. Besides, the solvent quality of the continuous phase of the emulsion
87 was modified to improve the emulsification process and increase the stability of the ATP
88 emulsion.

89 Polyols (including sugar alcohols) are known to change the solvent properties of water and
90 enhance hydrophobic interactions of proteins (Gekko, 1981; Cioci, 1995). They may also
91 influence water and protein solutions surface tension (Romero & Albis, 2010). These
92 information suggested that sugar alcohols can affect the interfacial tension and phase
93 equilibrium in ATP emulsions. Sugar alcohols are reduced form of sugars with an attached
94 alcohol group in substitution to the aldehyde. Postprandially, they cause only a small change
95 in blood sugar, which is especially beneficial for diabetics. However, ingestion of high
96 amounts of these compounds can lead to bloating and diarrhea (Marcus, 2013). As an
97 exception, erythritol is well (60–90%) and rapidly absorbed in the small intestine, which

98 makes it unlikely to observe the laxative side-effects associated with excessive consumption
99 of other sugar alcohols. Erythritol is excreted intact into urine and does not enter blood
100 circulation. Therefore, its glycemic index and caloric value are 0 and 0.2 kcal/g, respectively,
101 against 100 and 3.9 kcal/g for sucrose. Erythritol is roughly 70% as sweet as sucrose with no
102 after-taste (Grembecka, 2015). In addition to the conventional application as sweetener, sugar
103 alcohols have been studied for their solubility in ionic liquids in biorefinery processes
104 (Paduszyński, Okuniewski, Domańska, 2015), as phase-change materials for waste heat
105 management (Nomura, Zhu, Sagara, Okinaka, & Akiyama, 2015) and as starch plasticizer and
106 swelling inhibitory (Sun, Nan, Dai, Ji and Xiong, 2014).

107 The objective of the present study was to form ATP emulsions using a designed protein-rich
108 aqueous phase, made incompatible with alginate droplets. This dispersant would be composed
109 of hydrophobized whey protein (produced using a food-grade acetylating agent i.e. acetic
110 anhydride), and erythritol, which is a low-calorie and naturally occurring zero-glycemic index
111 sweetener. Interaction of protein particles with erythritol and the influence of erythritol on
112 solvent properties were assessed by several techniques to understand how protein
113 hydrophobization and erythritol addition synergistically favored ATP emulsion formation and
114 stability.

115 **2. Materials and methods**

116 *2.1. Materials*

117 Whey protein isolate (WPI) powder was kindly gifted by Lactalis ingredients (Lactalis Group,
118 Bourgbarré, France). It had 90% protein, 5.1% water, 3.0% lactose, and 1.97% ash contents in
119 weight. Erythritol was purchased from Vita-World GmbH (Taunusstein, Germany). All
120 chemicals used in the current study were analytical grade.

121 *2.2. Protein acetylation*

122 WPI solution (65 mg/mL) was hydrophobized by the procedure described elsewhere
123 (Madadlou et al., 2018) with minor modifications and used for emulsification. Briefly, WPI
124 solution (65 mg/mL) was titrated with acetic anhydride at an anhydride to protein ratio of
125 ≈ 0.18 g/g. This was followed by gradual titration of the solution with 1 M NaOH to keep pH
126 above 8.0 for 30 min. After the last titration, the WPI solution (pH ≈ 8.70) was heat-treated at
127 85°C for 20 min, which reduced pH to approximately 7.40. Heat-denatured (without
128 acetylation) and native (not heated nor acetylated) WPI samples at pH 8.70 were also
129 prepared and used in some experiments. The pH of the WPI samples was adjusted by either 1
130 M HCl (for native and heat-denatured samples) or NaOH (for hydrophobized sample) on to
131 8.30 ± 0.1 before emulsification.

132 2.3. Phase diagram

133 Different concentrations (0, 50, 100, 150, and 200 mg/g) of erythritol were added to the WPI
134 solutions (native, heat-denatured and hydrophobized) and dissolved by vortexing. Then, the
135 samples were supplemented with sodium alginate (1, 2, 3, 5, 7, 10, and 15 mg/g) and the
136 mixtures were shaken overnight at 500 RPM and 20°C . Subsequently, the mixtures were
137 centrifuged at $17,000 \times g$ for 30 min and the presence or absence of a fluid-fluid interface
138 visible by the naked eye was noted. The phase diagram was plotted on dry basis using the
139 triangular diagram of Extended UNIQUAC thermodynamic model (Thomsen & Rasmussen,
140 1999; Aqueous Solutions Aps, Søborg, Denmark) with Excel interface. The top and bottom
141 phases were separately collected and read at 278 nm (UV-visible spectrophotometer, model
142 UVmc2, SAFAS Monaco) to determine the protein- and alginate-rich phases.

143 2.4. Emulsification method

144 A series of preliminary tests were performed at different concentrations of WPI (35–65
145 mg/mL) and alginate (20–70 mg/mL), mixing speeds, mixing ratios of the two aqueous
146 solutions, as well as various concentrations of NaCl (0, 50 and 100 mM) in the WPI solution

147 and several concentrations of erythritol. Accordingly, native, heated and hydrophobized (i.e.
148 acetylated + heated) WPI samples (65 mg/mL) were supplemented with different
149 concentrations (0, 52, 105 and 158 mg/g) of erythritol. Then, sodium alginate solution (30
150 mg/mL) was added as disperse phase (0.1 g) into WPI-erythritol mixed solution (0.9 g) and
151 the mixture was vortexed at 40 Hz (Bioblock Top Mix 11118, Fisher Scientific, Waltham,
152 MA, USA) for 2 min to obtain the ATP emulsion. Alternatively, the protein-polysaccharide
153 mixtures were homogenized at a high shear rate (30,000 rpm, IKA T 10 basic ULTRA-
154 TURRAX, IKA[®]-Werke GmbH & Co. KG, Staufen, Germany) but no difference was
155 observed between the droplet size of emulsions prepared by either vortex agitator or high-
156 speed homogenizer. Therefore, vortex agitation was used in the remainder of the study.

157 *2.5. Protein particle diameter and electric charge*

158 WPI samples with added erythritol were diluted 100 folds in distilled water and the
159 hydrodynamic diameter and ζ -potential of protein particles were measured by dynamic light
160 scattering (DLS) using a Zetasizer Nano ZS (Malvern Instruments Ltd., Worcestershire, UK).
161 A laser wavelength of 633 nm at backscattering angle of 173° was applied for size
162 measurements at 20°C and 38°C. The results are intensity-averaged values unless stated
163 otherwise.

164 *2.6. Intrinsic fluorescence spectroscopy*

165 The peak fluorescence emission wavelength (λ_{em}) and intensity of WPI solutions were
166 measured using a cuvette spectrofluorometer (FLX-Xenius, SAFAS Monaco, Monaco). WPI
167 samples were diluted 100 folds with distilled water, then supplemented with different
168 concentrations of erythritol, at erythritol to WPI ratios of 0:1, 3:1, 6:1, 11:1, 13:1, 21:1, 24:1,
169 30:1, and 34:1 and excited at 290 nm. Emission spectra were recorded at 300–400 nm with
170 the entrance and exit slits set at 10 nm. The fluorescence intensity of water as blank was
171 subtracted to correct background fluorescence.

172 2.7. Viscosity measurement

173 Viscosity of WPI samples was measured using a rotational viscometer with coaxial cylinders
174 system (LS 400 rheometer, Lamy Rheology, Champagne-au-Mont-d'Or, France) at 20°C.
175 Samples were sheared over the range of 2–100 s⁻¹ and the obtained data were fitted to either
176 Newtonian (R₂≥0.999) or Power law (R₂≥0.999) models to determine their respective flow
177 behavior.

178 2.8. Atomic force microscopy imaging

179 Five µL of each suspension were spread over freshly cleaved mica (1×1 cm²) then put in a
180 dessicator for at least 4 days. Imaging of the dessicated samples was performed using a
181 MFP3D-BIO AFM (Asylum Research, Santa Barbara, CA, USA) operated in AC mode and at
182 room temperature, using AC240TS silicon probes (Olympus, spring constant $k \sim 2 \text{ N.m}^{-1}$, tip
183 radius $\sim 9 \text{ nm}$). The typical scan rate was 0.5-1 Hz (2-20 µm/s) for 256 × 256 pixel images.
184 The images were typically plane-fitted at order 0 then flattened at order 1. Sections were
185 drawn across images to measure the apparent basal width and height of individual objects on
186 the images.

187 2.9. Surface tension measurement

188 Surface tension of WPI solutions was measured at 20°C by using a pendant drop tensiometer
189 ('Tracker' from Teclis- Scientific, France). Drops of 7 µL were formed at the tip of a syringe
190 containing the protein solutions. The drop profile was determined by image analysis, from
191 which the surface tension was derived. Under mechanical equilibrium of capillary and gravity
192 forces, the Laplace equation relates the pressure difference across the interface, the surface
193 tension and the surface curvature.

194 2.10. Emulsion imaging

195 Emulsion samples were imaged at room temperature (20°C) using a phase contrast optical
196 microscope equipped with an epifluorescence module (Olympus BX51TF, Olympus,

197 Hamburg, Germany) set at the magnification $\times 100$. The imaging was carried out at non-
198 fluorescent (bright field light microscopy) and fluorescent modes. For fluorescent imaging, an
199 emulsion sample (90 μL) was stained with Fast Green FCF dye (1 w/v%, 10 μL) and imaged.
200 The mean diameter of droplets was calculated by measuring the diameter of 20-40 droplets in
201 each micrograph with Archimed software (version 7.1.1, Microvision Instruments, Evry
202 cedex, France).

203 *2.11. Statistical analysis*

204 Samples were fabricated at least three times and the experiments were triplicated. The results
205 were analyzed by One-way ANOVA with SPSS software version 16 (IBM software, NY,
206 USA) using Duncan's test at a significance level of $p < 0.05$.

207 **3. Results on emulsion formation and stability**

208 Native WPI and alginate formed homogenous protein-polysaccharide solutions at any
209 concentration of erythritol (Fig. 1A), which reveals the compatibility of native whey proteins
210 and alginate in our experimental conditions. Moreover, it has been demonstrated that native
211 whey proteins cannot stabilize the interface of two immiscible aqueous solutions (Nguyen,
212 Nicolai, & Benyahia, 2013). Considering that the expected interfacial tension should be
213 extremely low between two immiscible aqueous solutions as opposed to oil-water interfaces
214 ($\mu\text{N/m}$ to be compared to mN/m) (Ganley et al., 2017) and that the particle size of native
215 whey proteins is too small (Table 1), the adsorption energy of the protein on the interface
216 remains low. Hence, native protein particles cannot stabilize ATP emulsions (Esquena, 2016).
217 In agreement to our findings, mixing native WPI with co-charged polysaccharides
218 (carrageenan or pectin) did not yield ATP emulsions (Chun et al., 2014).

219 Heat-treatment of whey proteins has been shown to promote phase separation and ATP
220 formation (Thongkaew, Hinrichs, Gibis, & Weiss, 2015), which was attributed to the
221 mitigation of depletion flocculation, as more space is available for polysaccharide chains

222 between two approaching thermally-induced protein filaments than between a pair of
223 homogenous spheres of native whey proteins (Chun et al., 2014). However, unlike native WPI,
224 the mixed solution of heat-treated WPI and alginate at all erythritol concentrations was
225 homogenous (Fig. 1A). In the current study, heat treatment did not produce long filamentous
226 structures which are formed by heating at neutral pH (Chun et al., 2014), but yielded
227 monodisperse spherical nano-particles (Table 1, section 4.1). In contrast to native and heat-
228 denatured WPIs, hydrophobized (i.e. pre-acetylated and subsequently acetylated/heat-treated) WPI
229 solution was immiscible with alginate and formed ATP emulsion (Fig. 1B). However, the
230 dispersed phase droplets coalesced rapidly and the emulsion phase separated into two distinct
231 layers of protein and polysaccharide after 1 day. When the phase-separated samples were
232 shaken by hand, remixing occurred, which indicates that the segregative phase separation was
233 reversible. This reversibility has also been reported for a mixture of heat-denatured WPI and
234 polysaccharides (Chun et al., 2014).

235 Figure 2 illustrates the ternary phase diagram of hydrophobized WPI, alginate and erythritol.
236 The E-free and E-added WPI and alginate solutions were mixed, shaken and centrifuged. At
237 alginate concentrations between 2 and 5 mg/g WPI solution, the mixtures separated into an
238 upper phase rich in alginate and a lower phase rich in whey protein. However, at the alginate
239 concentration of 7 mg/g WPI solution, a gel-like bottom phase was formed concomitant with
240 the absence of the uppermost alginate phase. The supernatant (above the gel-like bottom
241 phase) had a lower protein concentration than the protein-rich phase of the samples phase
242 separated to two distinct liquid layers (data not reported). As well, the mass of the gel phase
243 increased with increasing alginate concentration (7–15 mg/g WPI dispersion). These indicate
244 that alginate structured to form the gel, entrapping protein. Formation of a bottom phase
245 sediment by centrifugation is advantageous at separation and purification practices using the
246 ATPS technique (Walker & Lyddiatt, 1998). A macroscopically monophasic solution was

247 obtained at the alginate concentration of 1 mg/g WPI dispersion. It is known that phase
248 separation of protein and polysaccharide mixtures occurs only if the concentration of the
249 biopolymers reaches relatively high values (Pacek, Ding, Nienow, & Wedd, 2000). The
250 emulsion produced for microscopic imaging had an alginate content of 3 mg/g erythritol-free
251 and erythritol-added hydrophobized WPI solution.

252 Erythritol addition into the hydrophobized WPI solution enhanced emulsion formation (Fig. 1
253 C & D). At the erythritol concentration of 52 mg/g, the droplet size was remarkably
254 heterogeneous and in addition to many small droplets ($\approx 1.0\text{--}3.0\ \mu\text{m}$), a few large drops (>10
255 μm) were observed in the microscopic images (Fig. 1C). Nonetheless, at the erythritol
256 concentration of 105 mg/g, a highly stable emulsion (for at least 1 week) with less
257 heterogeneous droplets (Fig. 1D) was produced. In Fig. 1C, the partial coalescence of two
258 large drops in the 1st day of emulsion preparation is shown for the sample prepared at the
259 erythritol concentration of 52 mg/g. Whereas, at 105 mg/g erythritol content, droplets evolved
260 much slower, and the mean size of the droplets only reached 5 μm after 1 week storage at
261 20°C (Fig. 1F). The time evolution is consistent with the usual Ostwald ripening of dilute
262 emulsions (with a size R scaling with time t such as $R \sim t^{1/3}$), which indicates that diffusion
263 between the alginate droplets contributed to the droplet size growth.

264 We identified by fluorescent microscopy imaging (Fig. 1G) that whey proteins formed the
265 continuous phase, while phase inversion and mixing of the aqueous phases did not occur over
266 storage of the emulsion. In contrast to the opaque and milky appearance of oil-water
267 emulsions, the ATP emulsions because of small difference in the refractive index of the two
268 aqueous phases (Singh et al., 2018) were rather transparent. A bi-continuous ATP emulsion
269 was obtained at the highest concentration (i.e. 158 mg/g) of erythritol (Fig. 1E).

270 **4. Complementary results: protein particles, bulk and interfacial properties**

271 At this stage, a variety of experiments were carried out to explain why WPI hydrophobization
272 caused ATP emulsion formation, and how the addition of erythritol to the hydrophobized WPI
273 solution helped to form the emulsion. However, one should keep in mind that erythritol would
274 partition between the WPI-rich and alginate-rich phases. Protein and alginate also partition
275 between the phases, which will result in complex multi-component phases. Therefore, the
276 information provided here mainly address the emulsification stage and further investigations
277 must be performed to describe the behavior of the emulsion over storage.

278 *4.1. Protein particle characteristics and viscosity*

279 The number-averaged particle diameter of the control native WPI was found to be
280 approximately 2.9 nm. Heating and hydrophobization (i.e. pre-acetylation and subsequent
281 acetylation/heating) processes resulted in formation of whey protein nano-particles of
282 approximately 57 and 80 nm Z-average diameter (which is the intensity-weighted arithmetic
283 average diameter of particles), respectively (Table 1). In DLS, the intensity decay rate Γ of the
284 scattered light is used to obtain the diffusion coefficient D of freely floating particles in a
285 suspension:

$$286 \quad \Gamma = q^2 D \quad \text{[Eq. 1]}$$

287 where q is the modulus of scattering vector. When qR becomes substantially larger than 1,
288 relaxation of particles internal structure contributes to Γ . In the current study, qR had a
289 maximum value of 1.2, indicating that the intensity relaxation derived mainly from the
290 particles Brownian motion. However, it is noteworthy that the z-average radius is
291 underestimated at values smaller than q^{-1} , which was 38 nm in this study. There was no
292 difference between the polydispersity indices of heat-denatured and hydrophobized particles.
293 Results on particle size, surface hydrophobicity and electric charge, free amino groups
294 content, and structural characteristics of the protein particles have been comprehensively
295 discussed elsewhere (Madadlou et al., 2018). Protein nano-particles made by either heating or

296 the hydrophobization process were slightly smaller at 38°C than 20°C (Table 1; $p < 0.05$).
297 Likewise, intrinsic viscosity and voluminosity data have suggested a slight shrinkage of
298 thermally treated whey proteins upon temperature increase (Eissa, 2013). The DLS method
299 calculates the hydrodynamic diameter of particles and takes account of the hydration layer
300 (Fissan, Ristig, Kaminski, Asbach, & Epple, 2014). Enhancement of the strength of the
301 constitutive hydrophobic interactions and/or partial dehydration of the protein particles could
302 decrease their Z-average diameter at the higher temperature. On the contrary, the mean
303 particle size of native whey proteins increased at 38°C in comparison to the ambient
304 condition. Increasing temperature to 38°C approximately doubled the particle size of native
305 whey proteins (Table 1; $p < 0.05$). We propose that hydrophobic interactions among the
306 partially unfolded protein monomers (in the alkaline conditions) were enhanced at the higher
307 temperature, resulting in dimer and multimer formation.

308 Sugar alcohols may interact with amino acids through hydrophilic-ionic (between $-OH$
309 groups of sugar alcohol and NH_3^+ and COO^- groups of amino acids), hydrophobic-
310 hydrophobic (between CH groups of sugar alcohols and non-polar side chains of amino acids)
311 and hydrophilic-hydrophobic interactions (Ali & Bidhuri, 2013). Nonetheless, erythritol
312 addition did not influence the Z-average diameter, polydispersity index and ζ -potential of
313 whey protein nano-particles at either 20°C or 38°C (Table 1), which suggests that erythritol
314 did not interact electrostatically with WPI particles. As well, the intrinsic fluorescence
315 emission peak (λ_{em}) and intensity of WPI samples were not influenced by erythritol addition
316 at different ratios of erythritol to WPI (Table 2). The shift of λ_{em} from 329 nm to 334 nm due
317 to heat treatment has been ascribed to whey protein denaturation and increased exposure of
318 Trp residues. Also, the bathochromic shift of λ_{max} due to hydrophobization was ascribed to a
319 less compact tertiary conformation of acetylated protein (Madadlou et al., 2018).
320 Fluorescence spectroscopy is a sensitive and rapid method to study molecular interactions

321 involving proteins. Measurement of intrinsic fluorescence quenching of a protein by ligands
322 allows assessment of the accessibility of quenchers to fluorophore groups of the protein,
323 mediated largely by hydrophobic forces (Zhang, Que, Pan, & Guo, 2008). Hydrophobic
324 interaction between a ligand and a protein decreases fluorescence intensity and may cause a
325 blue shift in the emission wavelength (Cui, Fan, Li, & Hu, 2004). The unchanged λ_{em} and
326 intensity (Table 2) indicates that erythritol did not interact hydrophobically with WPI
327 particles. In addition to concluding no interaction between erythritol and WPI particles, one
328 may assume (based on the DLS and intrinsic fluorescence results) that erythritol addition did
329 not influence interaction amongst the protein particles. Nonetheless, it is worth mentioning
330 that samples were diluted before DLS measurements; thus, the results do not reflect the
331 possible effect of erythritol on supramolecular organization of protein particles at a high WPI
332 concentration. Therefore, viscosity measurement was also used to probe the organization of
333 protein particles in non-diluted conditions.

334 As tabulated (Table 1), the viscosities of all WPI (native, heat-treated and hydrophobized)
335 samples without added erythritol were independent from shear rate, indicating that the
336 samples were Newtonian fluids. Identical rheological behavior has been reported for whey
337 protein concentrate (WPC) solutions (Benoit, Nor Afizah, Ruttarattanamongkol, & Rizvi,
338 2013). Heat treatment and hydrophobization increased the viscosity of WPI solution, due to
339 formation of larger nano-particles compared to native whey proteins (Table 1).

340 The flow property of WPI solutions was affected by erythritol addition (Table 1). Erythritol
341 addition (at 105 mg/g) caused an approximately 1.3-fold increase of the viscosity of native
342 and heat-treated WPI solutions but the samples kept a Newtonian behavior. Similarly, the
343 hydrophobized WPI solution with the lowest concentration of added erythritol (52 mg/g) had
344 Newtonian flow behavior and exhibited a higher viscosity than the counterpart without
345 erythritol. In contrast, addition of erythritol to hydrophobized WPI solution at concentrations

346 of ≥ 105 mg/g, changed the solution to a non-Newtonian fluid (Table 1). Although the
347 viscosity of hydrophobized WPI with 105 mg/g erythritol decreased with increasing shear rate
348 (Fig. 3), it always (at any shear rate) had a significantly higher viscosity than the native and
349 heat-treated samples with a comparable concentration of added erythritol. The shear thinning
350 property of the hydrophobized WPI solutions with ≥ 105 mg/g erythritol was weak (Won &
351 Kim, 2004). Non-ionic low-molecular weight osmolytes such as erythritol alter solvent
352 features and may cause steric crowding of biomacromolecules such as proteins due to
353 osmolytes exclusion from the protein surface (Ferreira, Breydo, Reichardt, Uversky &
354 Zaslavsky, 2016). It is also known that high concentrations of solutes because of excluding
355 water modulate protein-protein binding (Hassan & Steinbach, 2011). We hypothesize that
356 erythritol addition at a sufficiently high concentration (i.e. ≥ 105 mg/g) into WPI solution
357 caused macromolecular crowding of proteins, inducing interaction between hydrophobized
358 WPI nano-particles through their acetyl moieties. Direct interaction of solute (i.e. erythritol)
359 with proteins was not necessary to enhance the hydrophobic effect (Eggers & Valentine,
360 2001). The interactions between protein particles impaired the movement of water solvent at
361 low shear rates. Likewise, reduction of the micellization concentration of amphiphiles by
362 sugars has been ascribed to the enhancement of hydrophobic interactions (Kabir-ud-Din,
363 Khan, & Navqi, 2012).

364 4.2. AFM imaging

365 Although erythritol did not directly interact with WPI particles, it was hypothesized (from the
366 viscosity measurement results) that at the erythritol concentration of 105 mg/g, interactions
367 between hydrophobized protein particles were enhanced. AFM was applied to visualize
368 protein particles and acquire information about the influence of erythritol on the morphology
369 and association of WPI particles. Where erythritol (E) and native WPI (N) was deposited on
370 mica, the rugosity indicates some material on the mica; therefore, both erythritol and WPI

371 were adsorbed (Fig. 4, comparing E or N with mica) and no further step was required for the
372 successful immobilization of the objects.

373 Air-dried erythritol formed thick crystal-like structures of irregular shape and rugosity of tens
374 of nm order of magnitude (Fig. 4E). Similar irregular surfaces containing areas with pits and
375 asperities have been observed by tapping mode AFM imaging of lactose monohydrate and
376 erythritol (Traini, Young, Jones, Edge, & Price, 2006). Native WPI deposits showed rather
377 low rugosities (~2 nm; Fig. 4N) in agreement with other reports (Ikeda & Morris, 2002;
378 Demanèche, Chapel, Monrozier, Quiquampoix, 2009; Touhami & Dutscher 2008). Rugosity
379 of the WPI layer increased with heat denaturation and hydrophobization (acetylation/heating)
380 to reach 4-5 nm (Fig. 4H and A/H). In the AFM images, the dimensions of heat-denatured and
381 hydrophobized WPIs without erythritol (Fig. 4H and A/H) were much smaller than their
382 corresponding Z-average diameter (Table 1). Likewise, considerably shorter heights (only 11
383 nm) were estimated using AFM images for whey protein aggregates formed by heating than
384 what was expected from the results of light scattering studies (Ikeda, 2003). Ikeda & Morris
385 (2002) argued that vertical compression of proteins by the scanning probe of the microscope
386 accounts for the height reduction (approximately 40%) of native β -lactoglobulin particles. In
387 addition to the probe compression, particle deformation upon adsorption onto the mica can
388 decrease the height and increase the width of protein particles, especially that there was no
389 covalent binding (Silva, Bahri, Guyomarc'h, Beaucher, & Gaucheron, 2015). Finally,
390 dehydration of samples before AFM imaging probably shrunk the WPI particles. It is worth
391 mentioning that particles of hydrophobized WPI were more distinguishable at AFM images
392 than heat-denatured and native WPI particles (Fig. 4N, H and A/H). This suggests that
393 hydrophobized particles could retain their shape despite compression and flattening, and were
394 comparatively firmer than the other two samples.

395 A greater rugosity is observed for each sample in the presence of erythritol compared to
396 erythritol-free conditions (Fig. 4, compare N with N+E, H with H+E and A/H with A/H+E).
397 We argue that some erythritol scaffolds the WPI particles, helping them to retain their shape
398 upon drying. This hypothesis resembles the vitrification mechanism according which, an
399 amorphous glassy matrix is formed by sugars around proteins during drying, resulting in
400 preservation of the protein structure (Mensink, Frijlink, Maarschalk, & Hinrichs, 2017). Using
401 the visible height and width of individual particles seen on the images, the volume of the
402 corresponding spherical cap was calculated, from which the diameter of a sphere of
403 equivalent volume was deduced (Silva et al., 2015). A diameter value of 10–20 nm was
404 obtained for erythritol-added native (N+E) and heat-denatured (H+E) samples, against 150
405 nm for A/H+E (i.e. erythritol-added hydrophobized WPI). The latter is larger than the
406 corresponding Z-average diameter of the hydrophobized particles (Table 1) and may indicate
407 aggregates of particles, supporting our presumption that particles interacted by their acetyl
408 moieties.

409 *4.3. Surface tension of WPI solutions*

410 Data from the surface tension measurements are represented in Figure 5. Pure water
411 (containing NaN_3 at 100 mg/L to match the composition of WPI samples) had a surface
412 tension of approximately 73.1 mN/m. All WPI samples showed an initial rapid reduction in
413 surface tension, followed by a gradual decrease over time. It might require time periods as
414 long as 120 min to reach a constant surface tension value by protein solutions. Proteins
415 diffuse to the surface of freshly formed droplets, and then undergo conformational changes
416 and structural rearrangements (Kitabatake & Doi, 1982) to increase the number of contact
417 points at the air/water interface (Schröder, Berton-Carabin, Venema, & Cornacchia, 2017)
418 during surface aging, which reduces surface tension. The results (Fig. 5) obtained for native
419 and heat-denatured WPI samples are typical for proteins (Nylander, Hamraoui, & Paulsson,

420 1999). Heat-denaturation and hydrophobization decreased the surface tension of WPI
421 solution. The liquid-air interface is indeed a very hydrophobic surface (Chanasattru, Decker,
422 & McClements, 2008); hence, a lower surface tension value indicates a higher degree of
423 protein hydrophobicity. A correlation between surface activity and surface hydrophobicity has
424 already been observed for whey proteins (Schröder et al., 2017) and as expected,
425 hydrophobization (i.e. pre-acetylation and subsequent acetylation/heating combined process)
426 that caused a more significant increase in surface hydrophobicity of whey proteins than only
427 heating (Madadlou et al., 2018a) resulted in a greater reduction of surface tension. The surface
428 tension of hydrophobized WPI sample was approximately 48 mN/m after ageing of droplet
429 for 350 seconds. The results suggest that hydrophobized protein particles could adsorb to the
430 WPI-alginate interface, forming a layer that decreased the alginate droplets coalescence.

431 Erythritol addition to water (105 mg/g) caused a slight reduction of surface tension from
432 about 73 mN/m to 71.5 (Fig. 5), meaning that erythritol has a low surface activity. Similarly,
433 Yamada, Fukusako, Kawanami, Sawada, and Horibe (1997) observed that D-sorbitol (100
434 mg/g) decreased the surface tension of water from ≈ 73 mN/m to 70.1 mN/m at 20°C.
435 Evacuation of a number of erythritol molecules to the air-water interface due to the imperfect
436 fitting of the solute molecules within the tetrahedral structure of water (Brini et al., 2017)
437 explains the observed result.

438 Erythritol addition decreased the surface tension of native and heat-treated samples to
439 approximately that of hydrophobized WPI solution without added erythritol. As well, for the
440 hydrophobized WPI sample, we found that the higher the erythritol content, the lower the
441 surface tension (Fig. 5), so that, the surface tension values of hydrophobized WPIs with 105
442 and 158 mg/g erythritol were about 45 and 43.5 mN/m, respectively after ageing of droplet for
443 350 seconds. Therefore, the surface tension of the hydrophobized WPI solution decreased by
444 a value of 3 mN/m as a consequence of adding erythritol at 105 mg/g concentration, which is

445 an effect twice larger than what erythritol does on its own at the interface. Thus, the decrease
446 of surface tension, when erythritol is added, cannot be ascribed to a simple co-adsorption of
447 erythritol at the interface, together with whey proteins. As for viscosity, erythritol modifies the
448 interaction between particles, providing structures more hydrophobic. When a cosolvent is
449 added to an aqueous protein solution, chemical potentials of the cosolvent and protein are
450 mutually perturbed. Osmolytes such as sugars and polyols show a greater affinity to water;
451 thus, they are preferentially excluded from protein surface. This causes a negative
452 perturbation of the chemical potential of protein (Timasheff, 2002) which increases free
453 energy and renders the system thermodynamically more unfavorable. As the driving force of
454 protein adsorption to interface is the chemical potential gradient between the bulk and
455 interface, an increase in the chemical potential of the proteins in solution increases the
456 adsorption gradient, which can lead to an increased adsorbed amount of the protein onto air-
457 water interface (Abbas, Sharma, Patapoff, & Kalonia, 2012).

458 The dynamic surface tension of the WPI solution with added erythritol at the concentration of
459 158 mg/g was lower than that of the WPI sample with 105 mg/g erythritol during the whole
460 period of droplet aging. Nonetheless, the former failed to form an alginate-in-WPI emulsion
461 with discrete dispersed droplets (Fig. 1). Therefore, lower and lower surface tensions are not
462 the only requirements to make long-living emulsion. We argue that a balance between
463 viscosity and surface tension was essential to produce an ATP emulsion. The significantly
464 high viscosity of the WPI sample containing 158 mg/g erythritol prevented the Rayleigh-
465 Plateau instability, which usually leads to discrete droplets. Indeed, surface tension has to be
466 balanced by the viscous effects, which act during the emulsification.

467 We made an effort to measure the interfacial tension between the alginate and hydrophobized
468 WPI phases. However, the experiment failed because the alginate solution injected into the
469 hydrophobized WPI could not provide a typical shape, resulting from the balance between

470 surface tension and gravity (Fig. 6). The shape of rising or pending drops moving is
 471 characterized by the Bond number, which measures the balance between these interfacial and
 472 gravitational forces:

$$473 \quad Bo = \frac{\Delta\rho g L^2}{\gamma} \quad [Eq. 2]$$

474 where $\Delta\rho$, g , L^2 and γ are density difference between the disperse and surrounding phases
 475 (kg/m^3), gravitational acceleration (m/s^2), characteristic length (m), and interfacial tension
 476 (N/m), respectively.

477 The needle of the pendant drop tensiometer used in the current study had a section of 1 mm.
 478 Hence, the drops had a typical length scale L of 1 mm. At this scale, gravity turns out to be
 479 too strong to be balanced by surface tension, meaning that the interfacial tension of the two
 480 aqueous phases has to be in the range of $\mu\text{N/m}$, rather than the usual mN/m for oil-water
 481 emulsions. As a consequence, no stable drops could be made and the lighter fluid (i.e.
 482 alginate) simply raised upward. Nonetheless, the apparatus allowed us to observe that the two
 483 fluids were not spontaneously miscible; one can identify an interface between them (Fig. 6).
 484 The observed time evolution (Fig. 1F) consistent with the classical Ostwald ripening, is also
 485 an indirect signature of the existence of the interfacial tension between WPI and alginate (in
 486 the presence of erythritol). During emulsion formation, as the typical length scale of the
 487 generated drops was μm , the influence of interfacial tension was recovered. Indeed, the
 488 relevant quantity to estimate is γ/L , rather than only γ itself.

489 The interfacial stresses can also be compared to viscous ones by the Capillary number:

$$490 \quad Ca = \frac{\mu V}{\gamma} \quad [Eq. 3]$$

491 where μ and V are the fluid dynamic viscosity and velocity, respectively. It is observed in Fig.
 492 1E that when the interfacial stresses are too low compared to the viscous component, the

493 impact of having an interfacial tension vanishes and spherical drops (which are the signature
494 that surface tension plays a role) could not be created. Instead, in a viscous-dominated regime,
495 the elongated ligaments were formed. Lastly, we want to point out that the measurements of
496 the surface tension between WPI and air was still helpful, as it gave us important information
497 on how the hydrophobicity depended on the experimental conditions (presence of erythritol,
498 concentration, etc.).

499 **4. Summary and conclusion**

500 Hydrophobization of whey proteins was found effective to cause immiscibility of WPI
501 solution with alginate solution, but the resulting W/W emulsion was destabilized within 24 h.
502 Addition of erythritol strongly helped the emulsification and increased the stability of the
503 resulting emulsion. At the first glance, erythritol does not interact with WPI particles.
504 However, some further works are needed to fully understand the influence of erythritol on
505 WPI particles. It was concluded that erythritol addition into WPI solution enhanced
506 emulsification by a further increase of the hydrophobicity of the WPI particles, promoting
507 phase separation and the occurrence of a non-zero (but extremely low) surface tension
508 between the two phases. It also improved the emulsion stability by reducing droplets
509 coalescence due mainly to increased viscosity. Nonetheless, a balance between viscosity of
510 the continuous phase (WPI solution) and the interfacial tension was essential to accomplish
511 efficient emulsification because higher viscosities of the WPI phase prevented the
512 miniaturization of alginate phase. The developed ATP emulsion can serve as a delivery
513 vehicle of bioactive compounds and other ingredients to diabetics, obese and elderly people
514 because it does not contain oil and absorbable sweetener.

515 **Acknowledgements**

516 The authors are thankful to the support of the EU in the framework of the Marie-Curie FP7
517 COFUND People Programme, through the award of an AgreeSkills+ fellowship (grant
518 agreement n°609398).

519 The Asylum Research MFP3D-BIO atomic force microscope was funded by the European
520 Union (FEDER), the French Ministry of Education and Research, INRA, Conseil Général 35
521 and Rennes Métropole.

522 **References**

- 523 Abbas, S.A., Sharma, V.K., Patapoff, T.W., & Kalonia, D.S. (2012). Opposite effects of
524 polyols on antibody aggregation: Thermal versus mechanical stresses. *Pharmaceutical*
525 *Research*, 29, 683–694.
- 526 Ali, A. & Bidhuri, P. (2013). Solvation thermodynamics of xylitol in water and in aqueous
527 amino acids at 298.15 K. *Journal of Physical Organic Chemistry*, 26, 54-58.
- 528 Benoit, S. M., Nor Afizah, M., Ruttarattanamongkol, K., & Rizvi, S. S. H. (2013). Effect of
529 pH and temperature on the viscosity of texturized and commercial whey protein dispersions.
530 *International Journal of Food Properties*, 16, 322-330.
- 531 Brini, Fennell, Fernandez-Serra, Hribar-Lee, Lukšič, & Dill, K. A. (2017). How water's
532 properties are encoded in its molecular structure and energies. *Chemical Reviews*, 117,
533 12385–12414.
- 534 Chanasattru, W., Decker, E.A., & McClements, D.J. (2008). Impact of cosolvents (polyols) on
535 globular protein functionality: Ultrasonic velocity, density, surface tension and solubility
536 study. *Food Hydrocolloids*, 22, 1475–1484.
- 537 Chun, J.-Y., Hong, G.-P., Surassmo, S., Weiss, J., Min S.-G., & Choi, M.-J. (2014). Study of
538 the phase separation behaviour of native or preheated WPI with polysaccharides. *Polymers*,
539 55, 4379–4384.
- 540 Cioci, F. (1995). Catalytic activity of *Aspergillus niger* glucose oxidase in water-polyol
541 mixtures. *Catalysis Letters*, 35, 395–405.
- 542 Cui, F.-L., Fan, J., Li, J.-P., Hu, Z.-D. (2004). Interactions between 1-benzoyl-4-*p*-
543 chlorophenyl thiosemicarbazide and serum albumin: investigation by fluorescence
544 spectroscopy. *Bioorganic and Medicinal Chemistry*, 12, 151–157.
- 545 de Freitas, R.A., Nicolai, T., Chassenieux, C., & Benyahia, L. (2016). Stabilization of water-
546 in-water emulsions by polysaccharide-coated protein particles. *Langmuir*, 32, 1227–1232.
- 547 Demanèche, S., Chapel, J.-P., Monrozier, L. J., & Quiquampoix, H. (2009). Dissimilar pH-
548 dependent adsorption features of bovine serum albumin and α -chymotrypsin on mica probed
549 by AFM. *Colloids & Surface B: Biointerfaces*, 70, 226–231.

- 550 Dewey, D. C., Strulson, C. A., Cacace, D. N., Bevilacqua, P. C., & Keating, C. D. (2014).
551 Bioreactor droplets from liposome-stabilized all-aqueous emulsions. *Nature Communications*,
552 5, 4670.
- 553 Eggers, D. K., & Valentine, J. S. (2001). Crowding and hydration effects on protein
554 conformation: a study with sol-gel encapsulated proteins. *Journal of Molecular*
555 *Biology*, 314, 911–922.
- 556 Eissa, A.S. (2013). Newtonian viscosity behavior of dilute solutions of polymerized
557 whey proteins. Would viscosity measurements reveal more detailed molecular
558 properties? *Food Hydrocolloids*, 30, 200–205.
- 559 Esquena, J. (2016). Water-in-water (W/W) emulsions. *Current Opinion in Colloid &*
560 *Interface Science*, 25, 109–119.
- 561 Ferreira, L. A., Breydo, L., Reichardt, C., Uversky, V. N., & Zaslavsky, B. Y.
562 (2016). Effects of osmolytes on solvent features of water in aqueous solutions,
563 *Journal of Biomolecular Structure and Dynamics*, 35, 1055-1068.
- 564 Firoozmand, H., Murray, B.S., and Dickinson, E. (2009). Interfacial structuring in a
565 phase separating mixed biopolymer solution containing colloidal particles.
566 *Langmuir*, 25, 1300–1305.
- 567 Fissan, H., Ristig, S., Kaminski, H., Asbach, C., & Eppe, M. (2014). Comparison of
568 different characterization methods for nanoparticle dispersions before and after
569 aerosolization. *Analytical Methods*, 6, 7324-7334.
- 570 Ganley, W.J., Ryan, P.T., & van Duijneveldt, J.S. (2017). Stabilisation of water-in-
571 water emulsions by montmorillonite platelets. *Journal of Colloid & Interface*
572 *Science*, 505, 139–147.
- 573 Gekko, K. (1981). Mechanism of polyol-induced protein stabilization: Solubility of
574 amino acids and diglycine in aqueous polyol solutions. *Journal of Biochemistry*, 90,
575 1633–1641.
- 576 Grembecka, M. (2015). Sugar alcohols—their role in the modern world of
577 sweeteners: a review. *European Food Research and Technology*, 241, 1–14.
- 578 Grinberg, V.Ya., and Tolstoguzov, V.B. (1997). Thermodynamic incompatibility of
579 proteins and polysaccharides in solutions. *Food Hydrocolloids*, 11, 145–158.
- 580 Hassan, S. A., & Steinbach, P. J. (2011). Water-exclusion and liquid-structure forces
581 in implicit solvation. *Journal of Physical Chemistry B*, 115, 14668–14682.
- 582 Ikeda, S. (2003). Heat-induced gelation of whey proteins observed by rheology,
583 atomic force microscopy, and Raman scattering spectroscopy. *Food Hydrocolloids*,
584 17, 399–406.

- 585 Ikeda, S. & Morris, V. J. (2002). Fine-stranded and particulate aggregates of heat-
586 denatured whey proteins visualized by atomic force microscopy.
587 *Biomacromolecules*, 3, 382–389.
- 588 Kabir-ud-Din; Khan, A.B., & Navqi, A.Z. (2012). Solution and surface properties of
589 amphiphilic drug – nonelectrolyte systems. *Physics and Chemistry of Liquids*, 50,
590 478–494.
- 591 Kitabatake, N & Doi, E. (1982). Surface tension and foaming of protein solutions.
592 *Journal of Food Science*, 47, 1218-1221.
- 593 Madadlou, A., Flourey, J., and Dupont, D. (2018). Structural assessment and
594 oxidation catalytic activity of hydrophobized whey proteins. *Journal of Agricultural*
595 *& Food Chemistry*. 66 (45), 12025–12033, DOI: 10.1021/acs.jafc.8b02362
- 596 Marcus, J.B. (2013). *Carbohydrate Basics: Sugars, Starches and Fibers in Foods*
597 *and Health Healthy Carbohydrate Choices, Roles and Applications in Nutrition,*
598 *Food Science and the Culinary Arts*, IN Culinary Nutrition. Pages 149–187. Elsevier,
599 Tokyo.
- 600 Mensink, M. A., Frijlink, H. W., Maarschalk, K. v., & Hinrichs, W. L. J. (2017).
601 How sugars protect proteins in the solid state and during drying (review):
602 Mechanisms of stabilization in relation to stress conditions. *European Journal of*
603 *Pharmaceutics & Biopharmaceutics*, 114, 288–295.
- 604 Moschakis, T., Chantzios, N., Biliaderis, C.G., and Dickinson, E. (2018).
605 Microrheology and microstructure of water-in-water emulsions containing sodium
606 caseinate and locust bean gum. *Food & Function*, 9, 2840–2852.
- 607 Mytnyk, S., Olive, A.G.L., Versluis, F., Poolman, J.M., Mendes, E., Eelkema, R., and
608 van Esch J.H. (2017). Compartmentalizing supramolecular hydrogels using aqueous
609 multiphase systems. *Angewandte Chemie International Edition*, 56, 14923–14927.
- 610 Nomura, T., Zhu, C., Sagara, A., Okinaka, N., & Akiyama, T. (2015). Estimation of
611 thermal endurance of multicomponent sugar alcohols as phase change materials.
612 *Applied Thermal Engineering*, 75, 481–486.
- 613 Nguyen, B.T., Nicolai, T., & Benyahia, L. (2013). Stabilization of water-in-water
614 emulsions by addition of protein particles. *Langmuir*, 29, 10658–10664.
- 615 Nicolai, T. and Murray, B. (2017) Particle stabilized water in water emulsions. *Food*
616 *Hydrocolloids*, 68, 157–163.
- 617 Nylander, T., Hamraoui, A. and Paulsson, M. (1999). Interfacial properties of whey
618 proteins at air/water and oil/water interfaces studied by dynamic drop tensiometry,
619 ellipsometry and spreading kinetics. *International Journal of Food Science &*
620 *Technology*, 34, 573-585.

- 621 Pacek, A. W., Ding, P., Nienow, A. W. and Wedd, M. (2000). Phase separation and
622 drop size distributions in “homogeneous” Na-alginate/Na-caseinate mixtures.
623 *Carbohydrate Polymers*, 42, 401–409.
- 624 Padiuszyński, K., Okuniewski, M., & Domańska, U. (2015). Solid–liquid phase
625 equilibria in binary mixtures of functionalized ionic liquids with sugar alcohols: New
626 experimental data and modelling. *Fluid Phase Equilibria*, 403, 167–175.
- 627 Poortinga, A.T. (2008). Microcapsules from self-assembled colloidal particles using
628 aqueous phase-separated polymer solutions. *Langmuir*, 24, 1644–1647.
- 629 Romero, C.M. and Albis, A. (2010). Influence of polyols and glucose on the surface
630 tension of bovine α -lactalbumin in aqueous solution. *Journal of Solution Chemistry*,
631 39, 1865-1876.
- 632 Schröder, A., Berton-Carabin, C., Venema, P., & Cornacchia, L. (2017). Interfacial
633 properties of whey protein and whey protein hydrolysates and their influence on
634 O/W emulsion stability. *Food Hydrocolloids*, 73, 129-140.
- 635 Silva, N. N., Bahri, A., Guyomarc’h, F., Beaucher, E., & Gaucheron, F. (2015). AFM
636 study of casein micelles cross-linked by genipin: effects of acid pH and citrate. *Dairy
637 Science & Technology*, 95, 75-86.
- 638 Singh, P., Medronho, B., Miguel, M.G., and Esquena, J. (2018). On the
639 encapsulation and viability of probiotic bacteria in edible carboxymethyl cellulose-
640 gelatin water-in-water emulsions. *Food Hydrocolloids*, 75, 41–50.
- 641 Song, Y., Shimanovich, U., Michaels, T. C. T., Ma, Q., Li, J., Knowles, T. P. J., &
642 Shum, H. C. (2016). Fabrication of fibrillosomes from droplets stabilized by protein
643 nanofibrils at all-aqueous interfaces. *Nature Communications*, 7, 12934.
- 644 Spicer, C.D. and Davis, B.G. (2014). Selective chemical protein modification.
645 *Nature Communications*, 5, 4740.
- 646 Sun, Q., Nan, C., Dai, L., Ji, N., and Xiong, L. (2014). Effect of sugar alcohol on
647 physicochemical properties of wheat starch. *Starch/Stärke*, 66, 788–794.
- 648 Thomsen, K. & Rasmussen, P. (1999). Modeling of vapor–liquid–solid equilibrium
649 in gas–aqueous electrolyte systems. *Chemical Engineering Science*, 54, 1787–1802.
- 650 Thongkaew, C., Hinrichs, J., Gibis, M., & Weiss, J. (2014). Sequential modulation of pH and
651 ionic strength in phase separated whey protein isolate – Pectin dispersions: Effect on
652 structural organization. *Food Hydrocolloids*, 47, 21–31.
- 653 Touhami, A. & Dutcher, J. R. (2009). pH-induced changes in adsorbed β -lactoglobulin
654 molecules measured using atomic force microscopy. *Soft Matter*, 5, 220–227.
- 655 Traini, D., Young, P.M., Jones, M., Edge, S., & Price, R. (2006). Comparative study of
656 erythritol and lactose monohydrate as carriers for inhalation: Atomic force microscopy and in
657 vitro correlation. *European Journal of Pharmaceutical Sciences*, 27, 243–251.

- 658 Tyagi, R., & Gupta M. N. (1998). Chemical modification and chemical cross-linking for
659 protein/enzyme stabilization. *Biochemistry-Moscow*, 63, 334–344.
- 660 Walker, S. G., & Lyddiatt, A. (1998). Aqueous two-phase systems as an alternative process
661 route for the fractionation of small inclusion bodies. *Journal of Chromatography B:*
662 *Biomedical Sciences and Applications*, 711, 185–194.
- 663 Walstra, P. (2003). *Physical chemistry of foods*. New York: Marcel Dekker, (Chapter 6).
- 664 Won, D., & Kim, C. (2004). Alignment and aggregation of spherical particles in viscoelastic
665 fluid under shear flow. *Journal of Non-Newtonian Fluid Mechanics*, 117, 141-146.
- 666 Yamada, M., Fukusako, S., Kawanami, T., Sawada, I., & Horibe, A. (1997). Surface tension
667 of aqueous binary solutions. *International Journal of Thermophysics*, 18, 1483–1493.
- 668 Zhang, G., Que, Q., Pan, J., & Guo, J. (2008). Study of the interaction between icariin and
669 human serum albumin by fluorescence spectroscopy. *Journal of Molecular Structure*, 881,
670 132–138.
- 671
- 672

Table 1. Particle size and ζ -potential of protein particles and the viscosity (at 20°C and between 2-100 s⁻¹) of whey protein isolate (WPI) samples.

WPI sample ¹ + erythritol (mg/g) content	Particle size; PDI		ζ -potential (mV)	Flow behavior	Viscosity (mPas)
	20°C	38°C			
N + 0	2.9 ± 0.3	6.4 ± 1.4	-26.1 ^c ± 2.6	Newtonian	1.47 ^h ± 0.1
N + 105	2.9 ± 0.2	6.1 ± 1.8	-25.9 ^c ± 2.9	Newtonian	1.92 ^g ± 0.1
H + 0	62.1 ^{cd} ± 1.2; 0.24	60.1 ^{de} ± 1.41; 0.23	-34.8 ^b ± 1.1	Newtonian	2.07 ^f ± 0.1
H + 105	62.7 ^c ± 1.6; 0.24	58.5 ^c ± 1.77; 0.21	-33.9 ^b ± 2.0	Newtonian	2.72 ^e ± 0.1
A/H + 0	87.2 ^a ± 3.1; 0.23	82.6 ^b ± 2.6; 0.22	-40.2 ^a ± 1.9	Newtonian	4.90 ^b ± 0.15
A/H + 52	88.4 ^a ± 2.0; 0.22	82.6 ^b ± 1.7; 0.23	-40.4 ^a ± 2.4	Newtonian	5.23 ^a ± 0.1
A/H + 105	88.9 ^a ± 1.5; 0.23	82.9 ^b ± 2.0; 0.22	-40.8 ^a ± 1.6	Shear-thinning	See Fig. 3
A/H + 158	89.6 ^a ± 1.5; 0.23	83.1 ^b ± 0.8; 0.23	-40.2 ^a ± 1.2	Shear-thinning	See Fig. 3

¹ N = Native; H = Heated; A/H = Acetylated/heated (hydrophobized) WPI samples.

Means with different superscripts within a column differ significantly ($p < 0.05$).

Table 2. Intrinsic fluorescence emission peak (λ_{em}) and intensity of whey protein isolate (WPI) samples mixed with erythritol (E) at different ratios of E to WPI between 0:1 and 34:1.

WPI sample ¹ + erythritol (w/w%) content	λ_{em} (nm)	Emission intensity (A.U.)
N + 0	329 ± 0	44.1 ± 1.2
N + E	329 ± 0	44.3 ± 1.6
H + 0	334 ± 0	13.7 ± 0.3
H + E	334 ± 0	14.4 ± 1.0
A/H + 0	335 ± 0	25.5 ± 0.9
A/H + E	335 ± 0	23.6 ± 0.8

¹ N = Native; H = Heated; A/H = Acetylated/heated (hydrophobized) WPI samples.

Figure captions

Fig. 1. Light microscopy images of alginate (30 mg/mL) and whey protein isolate (WPI) mixed solutions with added erythritol. All samples contained alginate solution at 10 w/w %.

The image A is an exemplar image showing homogenous solutions of alginate and either native or heat-denatured WPI supplemented with erythritol (0–158 mg/g).

The images B, C, D and E show emulsions of alginate-in-hydrophobized (acetylated and heat-treated) WPI containing 0, 52, 105 and 158 mg/g erythritol, respectively.

The image F plots droplet size of the alginate-in-hydrophobized WPI emulsion with 105 mg/g added erythritol over storage for 1 week and the solid line is a power law fit (t^a), and the fitting exponent is $a = 0.35$.

The image G shows exemplar epi-fluorescent microscopy images of the emulsion containing 105 mg/g erythritol at day 7.

Fig. 2. Phase diagram of hydrophobized protein (acetylated and heat-treated whey protein isolate), sodium alginate and erythritol after centrifugation. The hatched area confining the circles identifies combinations of the components that yielded immiscible liquid-liquid phases. The cubes indicate the combinations that yielded a gel-like bottom phase and a liquid supernatant phase, and the triangle indicates the combination that yielded a mono-phasic solution. The phase diagram was plotted on dry basis.

Fig. 3. Viscosity vs. shear rate ($\dot{\gamma}$) of hydrophobized whey protein isolate (A/H WPI) solutions supplemented with erythritol at 105 mg/g and 158 mg/g WPI solution. The measurement were carried out at 20°C; lines are power law fits, providing the values of n and K (respectively, the flow index and the consistency coefficient of the samples).

Fig. 4. Atomic force microscopy images. Aspect of dessicated deposits of native (N), heated (H) and acetylated/heatd (A/H) whey protein samples (65 g/L) spread onto mica (shown as control image), in absence (left) and presence (right) of 105 mg/g erythritol (E). Typical 2D and 3D topographical images as well as a typical 1- μ m cross-section are shown for each type of sample. Mind the scales which can differ, especially for E and A/H+E.

Fig. 5. Surface tension of whey protein isolate (WPI) solutions as a function of time. N, H and A/H abbreviate native, heat-denatured and hydrophobized (acetylated/heatd) WPI samples, respectively and the values report the concentration of erythritol (mg/g) added into WPI samples.

Fi. 6. The image of an alginate drop injected by a needle of the pendant drop tensiometer into the hydrophobized whey protein isolate (WPI) phase.

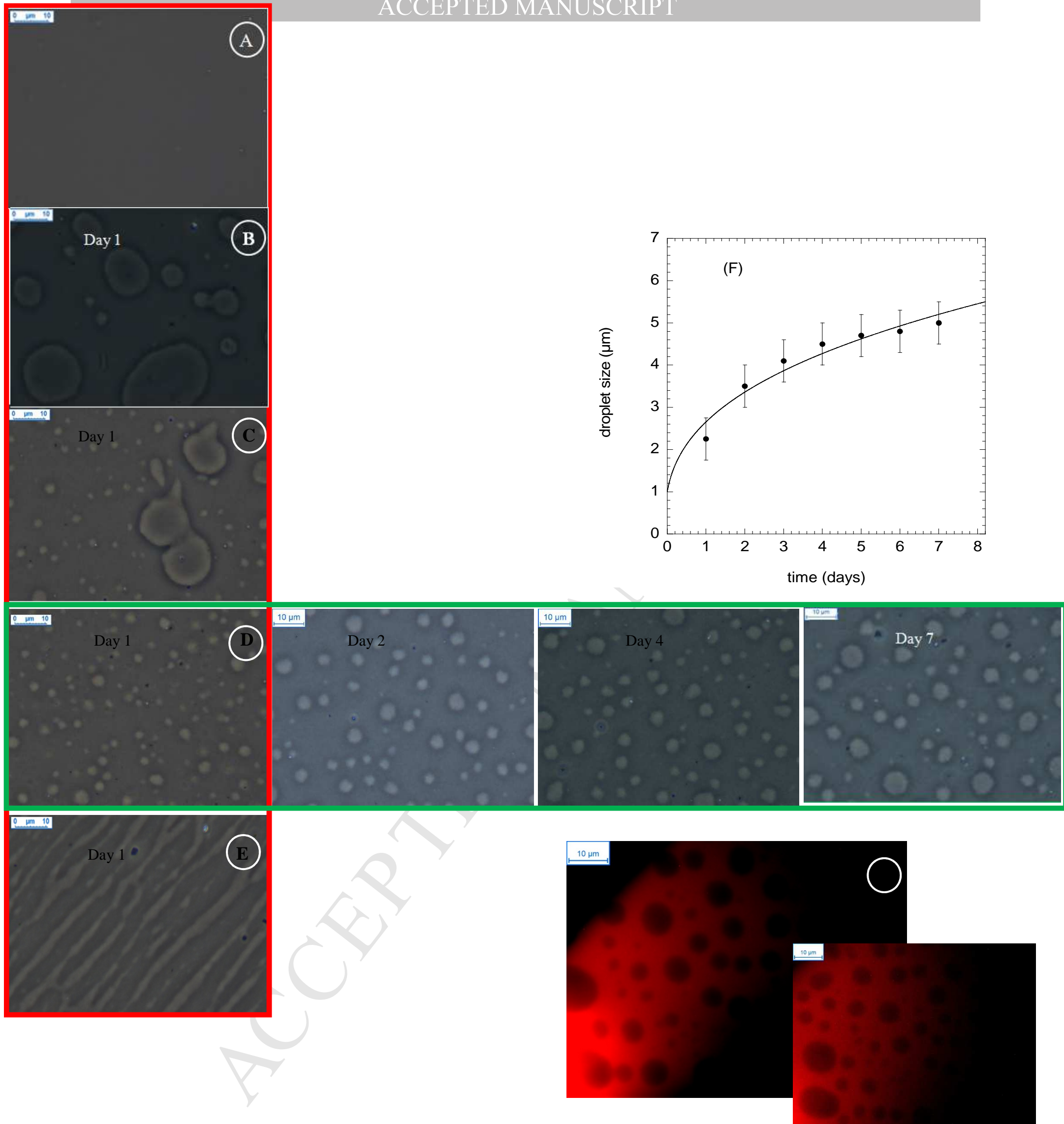


Figure 1.

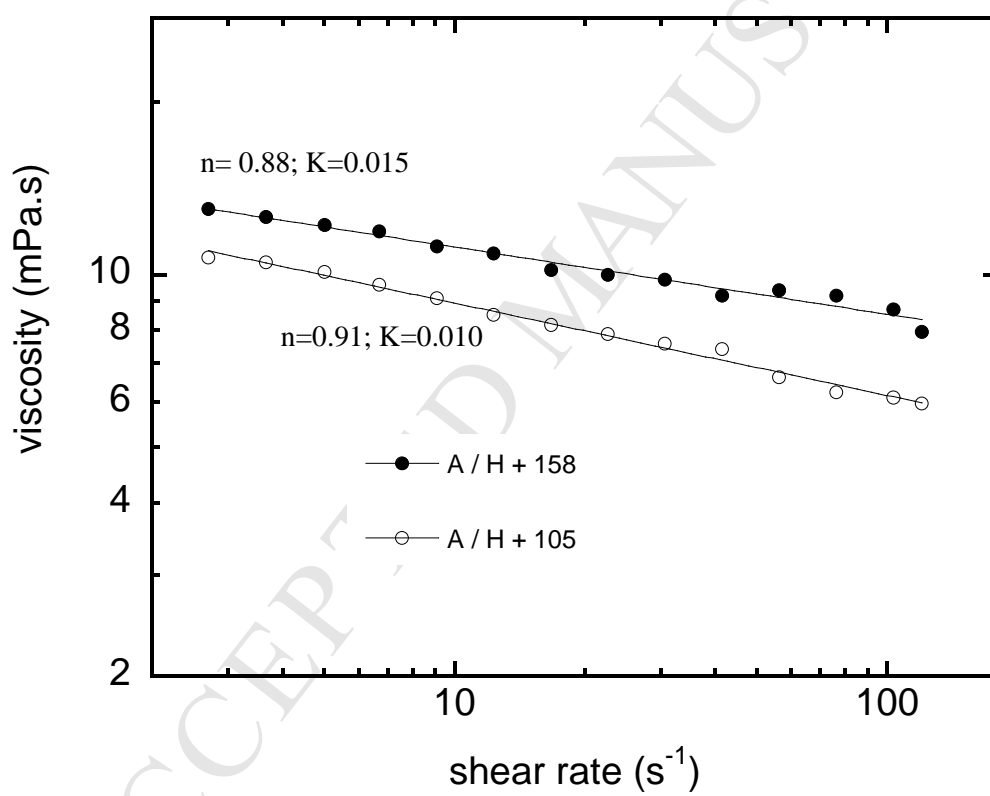


Figure 3.

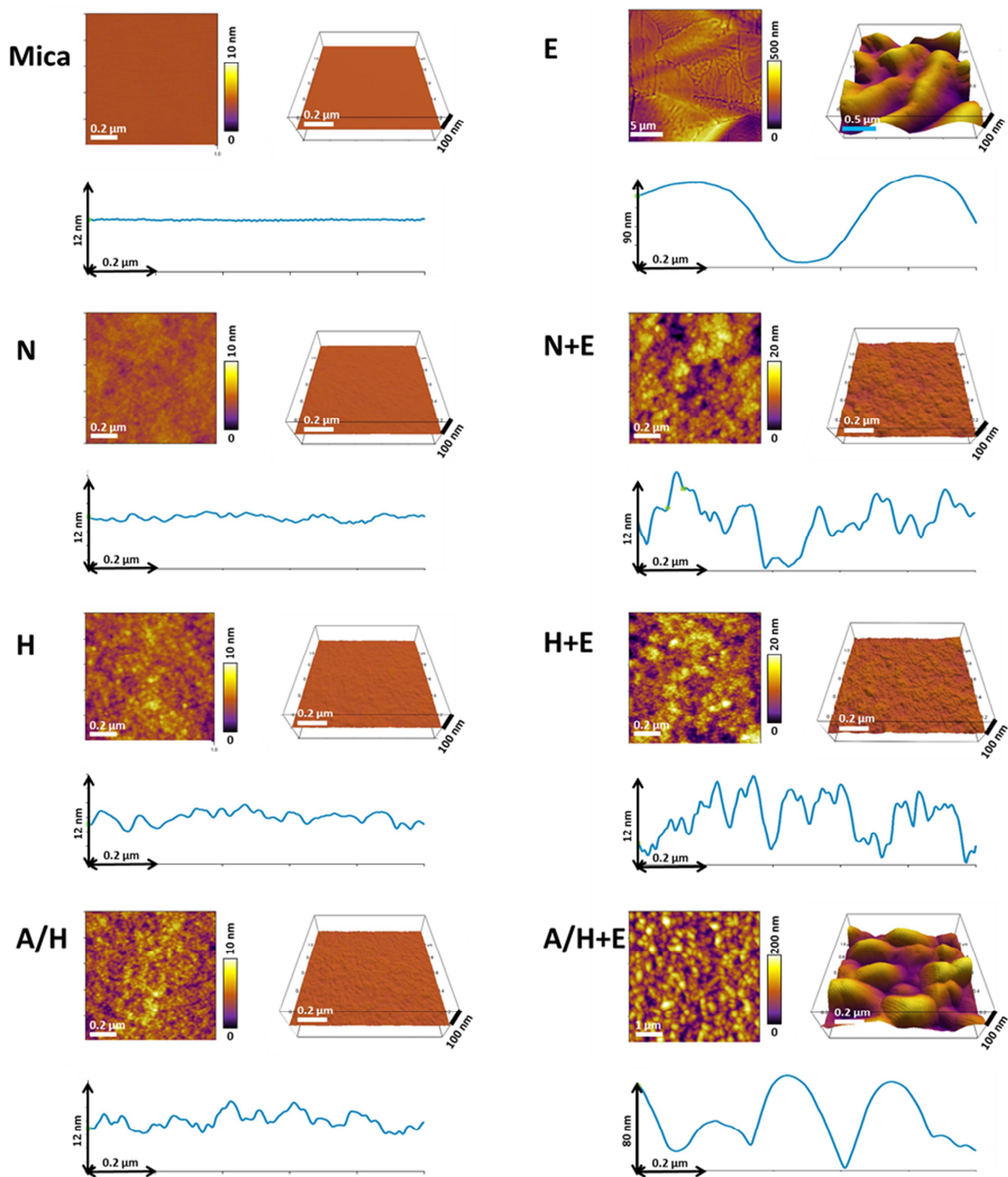


Figure 4.

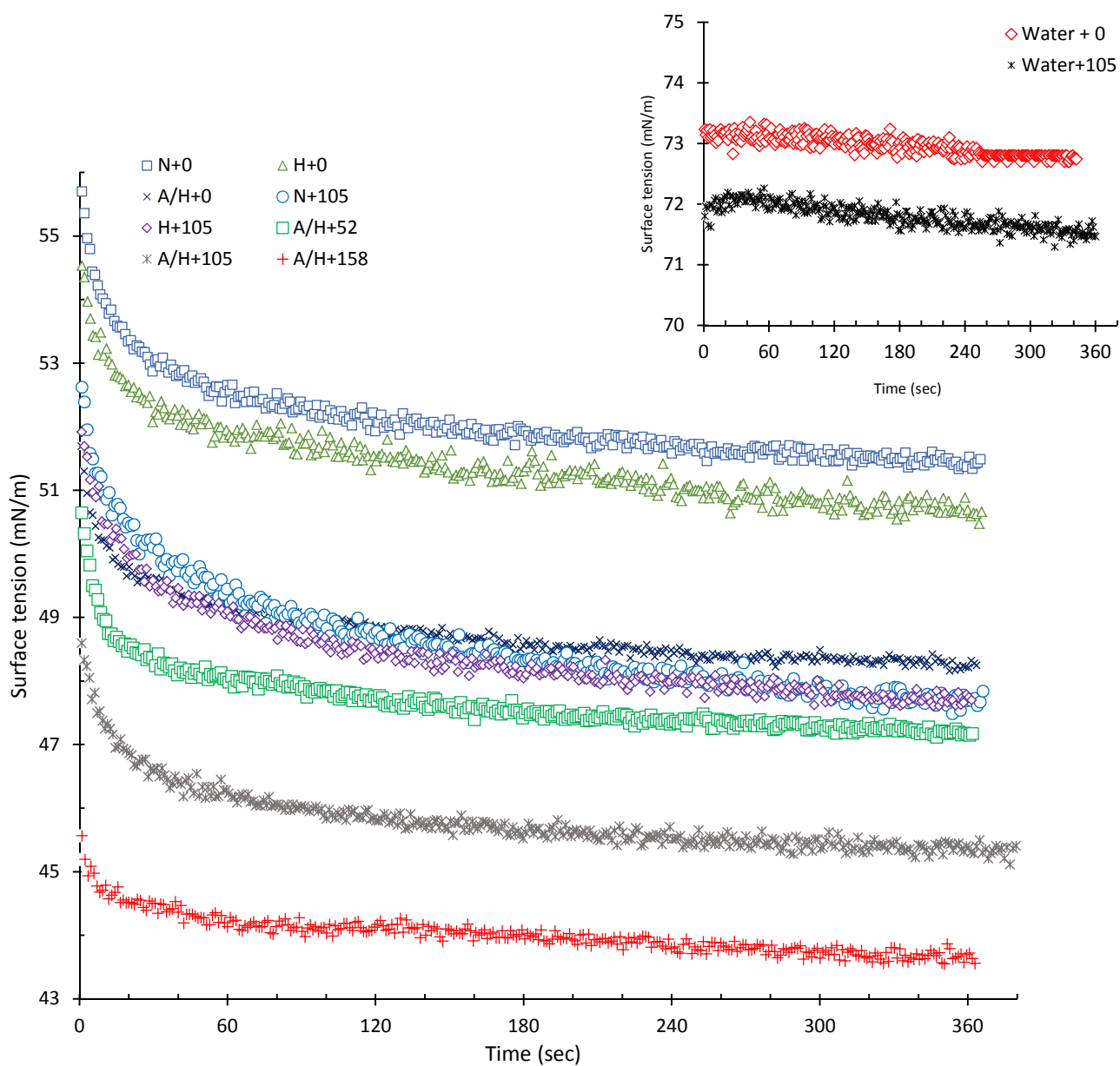


Figure 5.

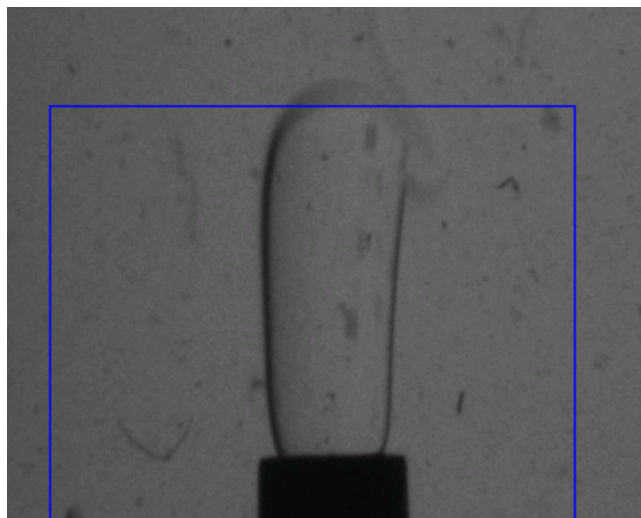


Figure 6.

